

Entropy drives protein conformational distributions in native globular proteins

Kai Wang¹ and Pu Tian^{1,2}

¹College of Life Science

²Key Laboratory of Molecular Enzymology and Engineering of the Ministry of Education, Jilin University, 2699 Qianjin Street, Changchun China 130012

August 23, 2018

Abstract

Protein conformational transitions, which are essential for function, may be driven either by entropy or enthalpy when molecular systems comprising solute and solvent molecules are the focus[1, 2]. Revealing thermodynamic origin of a given molecular process is an important but difficult task, and general principles governing protein conformational distributions remain elusive. Here we demonstrate that when protein molecules are taken as thermodynamic systems and solvents being treated as the environment, conformational entropy is an excellent proxy for free energy and is sufficient to explain protein conformational distributions. Specifically, by defining each unique combination of side chain torsional state as a conformer, the population distribution (or free energy) on an arbitrarily given order parameter is approximately a linear function of conformational entropy. Additionally, span of various microscopic potential energy terms is observed to be highly correlated with both conformational entropy and free energy. Presently widely utilized free energy proxies, including minimum potential energy[3, 4, 5], average potential energy terms by themselves[6] or in combination with vibrational entropy[7], are found to correlate with free energy rather poorly. Therefore, our findings provide a fundamentally new theoretical base for development of significantly more reliable and efficient next generation computational tools, where the number of available conformers, rather than potential energy of microscopic configurations, is the central focus. We anticipate that many related research fields, including structure based drug design and discovery, protein design, docking and prediction of general intermolecular interactions involving proteins, are expected to benefit greatly.

Protein molecules realize their function through proper distributions and dynamic transitions among hierarchically organized conformational substates. has both an entropic (S) and an enthalpic (H) component as indicated by the equation $G = H - TS$. Decomposing free energy change into entropic and enthalpic contributions of system comprising components and their correlations in typical biomolecular systems is critical for both their understanding and, more importantly, intervention and innovative design. However, this is extremely challenging and has not been rigourously realized for any realistic biomolecular systems. Isothermal Titration Calorimetry (ITC)[8] is an effective experimental means to split the total free energy change into entropic and enthalpic contributions, but further splitting of contributions into system-comprising components and their correlations is not possible. Computationally, rigorous methodologies based on free energy perturbation and thermodynamic integration[9] are expensive on the one hand, and do not provide entropic and enthalpic contributions on the other hand. Enthalpic contributions from any system-comprising components and their interactions are relatively easy to evaluate by molecular dynamics (MD) or Monte Carlo simulations. Calculating entropic contributions has been a major target of methodological development, and numerous statistical mechanical methods have been developed to calculate configurational entropy of either macromolecules[10, 11, 12, 13, 14, 15, 16, 17] or solvents[18, 19, 20]. Entropy reduction due to solvent-solute correlations remains a mystery, however. A number of free energy proxies have been utilized to overcome these challenges in computational studies. Typical examples include minimum potential energy by itself or in combination with conformational entropy in protein design, docking and structural refinement stage of folding[3, 21, 22, 5], linear combinations of average potential energy terms in linear interaction energy (LIE) model[6], and average potential energy terms together with vibrational entropy in MM-P/GBSA methodologies[7]. Here we choose protein molecules as thermodynamic systems to avoid difficulty of accounting for solvent contributions, especially the entropy reduction from solute-solvent correlations. When experimental measurements are used as benchmarks, methodological errors is always entangled with that caused by inaccuracy of force fields and insufficiency of sampling. By comparing free energy derived from population distributions with various free energy proxies obtained from the same set of MD simulation trajectories, inaccuracy of force fields and sampling limitation are effectively excluded. We evaluated reliability of potential free energy proxies, and conformational entropy in particular in light of its significance revealed by a number of experimental studies[23, 24]. It is found that conformational entropy, which has not been considered by itself as a free energy proxy, has the strongest linear correlation with free energy among all investigated energetic and entropic terms.

By dividing the whole configurational space into N_{conf} independent conformers, configurational entropy may be split into conformational and vibrational contributions such that[25, 26]:

$$S_{config} = S_{conf} + S_{vib} \quad (1)$$

$$S_{conf} = -k_B \sum_{i=1}^{N_{conf}} P(i) \ln P(i) \quad (2)$$

$$S_{vib} = \frac{1}{N_{conf}} \sum_{i=1}^{N_{conf}} S_{vib}^i \quad (3)$$

with $P(i)$ and S_{vib}^i being the probability and vibrational entropy of the conformer i respectively. Direct application of this equation, which implies complete sampling of the whole conformational space, is not feasible. Therefore, conformational entropy S_{conf} and vibrational entropy S_{vib} are calculated and analyzed separately.

In a series of studies[27, 28], Wand and coworkers found that local dynamics of methyl bearing side chains may serve as a robust entropy meter for conformational entropy of proteins. We were inspired to define each unique combination of torsional states for side-chain-heavy-atom (SCHA) defined torsional degree of freedom (DOF) (including χ_1) as an independent conformer. A torsional state is defined by a local maximum in the distribution of the corresponding torsion angle. For a given protein, two structural states belong to the same conformer only when each pair of their corresponding SCHA torsional DOFs are in the same torsional state. We assigned snapshots from MD trajectories of hen egg white lysozyme (HEWL)[29] ($200\mu s$ with 50,000,000 snapshots) and bovine pancreatic trypsin inhibitor (BPTI)[30] ($\sim 1ms$ with 4,124,963 snapshots) to unique conformers as defined above. The overwhelming majority of conformers were recorded only once (49348379 out of 49668320 for HEWL and 4124917 out of 4124940 for BPTI). Consequently, when projected onto an arbitrary order parameter that is divided into n windows, the number of snapshots in each window (N_i) is approximately equal to the corresponding number of conformers (N_{conf}^i). The net free energy and conformational entropy differences (ΔG^{ij} and ΔS_{conf}^{ij}) between two positions (i, j) on a given order parameter may be written as:

$$\Delta G^{ij} = -RT \ln\left(\frac{N_j}{N_i}\right) \quad (4)$$

$$\Delta S_{conf}^{ij} \approx R \ln\left(\frac{N_{conf}^j}{N_{conf}^i}\right) \quad (5)$$

$$\Delta G^{ij} \approx -T \Delta S_{conf}^{ij} \quad (6)$$

At the given time scale resolutions ($250ps$ for BPTI and $4ps$ for HEWL), vibrations within each defined conformer is barely seen explicitly and conformational entropy seems to represent free energy very well. Similar conclusions were obtained in analysis of two additional sets of MD trajectories (See supporting info). The assumption that all conformers have the same statistical weight as

in eq (5) may become problematic with higher resolution trajectories. To resolve this potential concern, we generated 20,000 10-*ps* trajectories for HEWL with their origins uniformly distributed in the original 200 μ s trajectories. The interval for saving snapshots is set to be 10*fs*, which is comparable with typical bonding vibrational cycles and are expected to capture interesting transitions within the visited configurational space. At this time scale resolution, conformers were found to have more heterogeneous distributions of statistical weight as shown in Fig. 1a, and motions within each conformer are treated as vibrations. Backbone dihedrals were first selected as order parameters to analyze the relationship between free energy and several entropic and energetic terms, including conformational entropy (S_{conf}) and its uniform distribution (upper bound) approximation ($\ln N_{conf}$), vibrational entropy (S_{vib}), minimum (E_{min}), maximum (E_{max}), average (E_{avg}) and span ($E_{span} = E_{max} - E_{min}$) of three potential energy terms (protein self energy E^p ; protein-solvent interaction energy E^{p-w} and their sums $E^{p+(p-w)}$). As shown in Fig. 1c, S_{conf} is found to be nearly linear with free energy on all backbone dihedrals, their linear correlation coefficients (r) range from -0.999 to -0.970 among 256 backbone dihedrals. Despite various statistical weight of conformers, $\ln N_{conf}$ is found to have nearly perfect linear relationship with free energy, with r distributed between -0.99 and -1.00 (See Fig. 1i). This quantity may be of great use for practical sampling algorithms, where determining statistical weight of each conformer can be difficult and costly. Surprisingly, E_{max}^p is found to correlate with free energy as significantly as E_{min}^p (Fig. 1e, 1f, 1j). E_{span}^p has the second best correlation with free energy (Fig. 1h, 1j). From a practical point of view, E_{span}^p may be incorporated, with virtually no additional cost, into any present sampling methodology that utilizes minimum potential energy as the free energy proxy, and improve its reliability. Both E_{avg}^p and S_{vib} are found to correlate poorly with free energy (Fig. 1g, 1i). Additionally, E_{min}^p (Fig. 1b) and E_{max}^p (Fig. S2) correlate consistently well with free energy on backbone dihedrals located in stable secondary structures, but their performance vary significantly (ranging from $r \sim 0.85$ to $r \sim 0.1$) on backbone dihedrals located in flexible region, which are more relevant in protein conformational transitions. E_*^{p-w} and $E_*^{p+(p-w)}$ exhibit similar correlation pattern with free energy as that is observed for E_*^p (with * representing *max*, *min*, *avg* or *span*, see Fig. S3-5). Statistical weights for conformers were found to correlate significantly with vibrational entropy (Fig. S6) and *span* of potential energy terms (Fig. S7) but correlate poorly with *max*, *min* and *avg* of potential energy terms (Fig. S7). In practice, strong linear correlation between $\ln N_{conf}$ and free energy renders calculation of conformers' statistical weight unnecessary.

Next, the same set of energetic and entropic terms were projected onto two other widely utilized order parameters, radius of gyration (R_g) and number of native contacts (NC), both are not representable as linear combinations of backbone torsional DOFs. The same order of correlation strength with free energy is found for S_{conf} , $\ln N_{conf}$, S_{vib} , E_{min}^p , E_{max}^p , E_{avg}^p and E_{span}^p (See Fig. 2(a-g) for projection on R_g and Fig. 2(h-n) for projection on NC). In folding, design

and docking studies, fitness of backbone configurations are evaluated by repetitively packing side chains and search for ones that have lowest energy according to given scoring functions, which usually are combinations of potential energy terms and solvation term. We clustered snapshots in 10-*fs*-interval trajectories according to their backbone torsional states, and each cluster is treated as a single window to investigate correlations between free energy and the same set of energetic and entropic terms analyzed above. As shown in Fig. 2(o-u), the same order of correlation strength with free energy is observed for $\ln N_{conf}$, S_{conf} , S_{vib} , E_{min}^p , E_{max}^p , E_{avg}^p and E_{span}^p on these clusters as that of other investigated order parameters. E_*^{p-w} and $E_*^{p+(p-w)}$ (with * representing *max*, *min*, *avg* or *span*) exhibit similar pattern of correlations with free energy as that of E_*^p (Fig. S8). While the performance of S_{conf} and $\ln N_{conf}$ deteriorate slightly on these backbone dihedral defined clusters when compared with projection on other order parameters, they are far and away superior to all of the energetic terms and vibrational entropy.

Protein conformational entropy has been considered in a number of computational algorithms[21, 22]. However, its utility as an excellent free energy proxy has not been revealed in these studies. The reason is that full solute-solvent molecular systems are selected as target of thermodynamic analysis. Consequently, the strong correlation between conformational entropy and free energy is camouflaged by large variations in potential energy and solvation terms, which are much larger in value than conformational entropy of proteins. Combination of average potential energy terms (E_{avg}^p and $E_{avg}^{p+(p-w)}$) with S_{vib} does not improve correlation with free energy in any considerable way (Fig. S9-10).

Given the observed monotonic map between conformational entropy and free energy, changing the number of available conformers is the most important path through which change of molecular interactions contributes to the change of free energy, which may consequently be rewritten as:

$$\Delta G^{protein} \propto -T \Delta S_{conf}^{protein} (\Delta H^{protein+solvent}) \quad (7)$$

for native globular proteins. The findings suggest that for studied proteins, conformational change are driven by conformational entropy. This conclusion is likely to be true for other globular proteins. Rough treatment of conformational entropy is a significantly underappreciated source of error in *enthalpy centric* computational algorithms (see supporting info) when compared to accuracy of force fields, which might have taken much undeserved blame.

methods

BPTI trajectories were provided by DE Shaw[30]. MD trajectories of HEWL (collectively 200 μs comprising 2000 100-*ns* trajectories) were taken from our previous simulation study[29]. 10 parallel 500-*ns* trajectories[31] were analyzed

for both barstar (started from pdb code 1bta) and ribonuclease (started from pdb code 1rgh). 20,000 10 f s-interval HEWL trajectories (collectively 200ns) were generated with NAMD[32] under the same conditions as in the previous study[29]. Backbone based clusters are constructed by using the established standard of $T4$ time scale in the same study[29]. Order parameters (including backbone dihedrals, radius of gyration and number of native contacts) are divided into 20 equally-sized windows to perform projection of various energetic and entropic terms. Fitting of various energetic and entropic terms as a linear function of free energy is performed by using linear least squares regression. Vibrational entropy was calculated with the Schlitter formula[10]. Potential energy terms were calculated with the NAMD pair interaction option.

Acknowledgements

This research was supported by National Natural Science Foundation of China under grant number 31270758. Computational resources were partially supported by High Performance Computing Center of Jilin University, China. We thank DE Shaw Research for providing BPTI trajectories.

References

- [1] Deng, N.-j., Zhang, P., Cieplak, P. & Lai, L. Elucidating the energetics of entropically driven protein-ligand association: calculations of absolute binding free energy and entropy. *The journal of physical chemistry. B* **115**, 11902–10 (2011). URL <http://www.ncbi.nlm.nih.gov/pubmed/21899337>.
- [2] Fenley, A. T., Muddana, H. S. & Gilson, M. K. Entropy-enthalpy transduction caused by conformational shifts can obscure the forces driving protein-ligand binding. *Proceedings of the National Academy of Sciences of the United States of America* **109**, 20006–11 (2012). URL <http://www.pubmedcentral.nih.gov/articlerender.fcgi?artid=3523842&tool=pmcentrez&render>
- [3] Desmet, J., Maeyer, M. D., Hazes, B. & Lasters, I. The dead-end elimination theorem and its use in protein side-chain positioning. *nature* **356**, 539–542 (1992).
- [4] Canutescu, A. A., Shelenkov, A. A. & Dunbrack, R. L. A graph-theory algorithm for rapid protein side-chain prediction. *Protein Science* **12**, 2001–2014 (2003). URL <http://dx.doi.org/10.1110/ps.03154503>.
- [5] Leaver-Fay, A. *et al.* Chapter nineteen - rosetta3: An object-oriented software suite for the simulation and design of macromolecules. In Johnson, M. L. & Brand, L. (eds.) *Computer Methods, Part C*, vol. 487 of *Methods in Enzymology*, 545 – 574 (Academic Press, 2011). URL <http://www.sciencedirect.com/science/article/pii/B9780123812704000196>.
- [6] Hansson, T., Marelus, J. & qvist, J. Ligand binding affinity prediction by linear interaction energy methods. *Journal of Computer-Aided Molecular Design* **12**, 27–35 (1998).
- [7] Kuhn, B. & Kollman, P. A. Binding of a diverse set of ligands to avidin and streptavidin: an accurate quantitative prediction of their relative affinities by a combination of molecular mechanics and continuum solvent models. *Journal of Medicinal Chemistry* **43**, 3786–3791 (2000). URL <http://pubs.acs.org/doi/abs/10.1021/jm000241h>. <http://pubs.acs.org/doi/pdf/10.1021/jm000241h>.
- [8] Falconer, R. J., Penkova, A., Jelesarov, I. & Collins, B. M. Survey of the year 2008: applications of isothermal titration calorimetry. *Journal of molecular recognition : JMR* **23**, 395–413 (2010). URL <http://www.ncbi.nlm.nih.gov/pubmed/20213668>.
- [9] Chipot, C. & Pohorille, A. *Free Energy Calculations, Theory and Applications in Chemistry and Biology* (Springer, Berlin Heidelberg New York, 2007).
- [10] Schlitter, J. Estimation of absolute and relative entropies of macromolecules using the covariance matrix.

- Chemical Physics Letters* **215**, 617–621 (1993). URL <http://www.sciencedirect.com/science/article/pii/000926149389366P>.
- [11] Tidor, B. & Karplus, M. The contribution of cross-links to protein stability: A normal mode analysis of the configurational entropy of the native state. *Proteins: Structure, Function, and Bioinformatics* **15**, 71–79 (1993). URL <http://dx.doi.org/10.1002/prot.340150109>.
 - [12] Andricioaei, I. & Karplus, M. On the calculation of entropy from covariance matrices of the atomic fluctuations. *The Journal of Chemical Physics* **115**, 6289 (2001). URL <http://link.aip.org/link/JCPSA6/v115/i14/p6289/s1&Agg=doi>.
 - [13] Hnizdo, V. *et al.* Nearest-Neighbor Nonparametric Method for Estimating the Configurational Entropy of Complex Molecules *. *Journal of computational chemistry* **28**, 655–668 (2006).
 - [14] Ohkubo, Y. Z. & Thorpe, I. F. Evaluating the conformational entropy of macromolecules using an energy decomposition approach Evaluating the conformational entropy of macromolecules using an energy. *Journal of Chemical Physics* **124**, 024910 (2006).
 - [15] Nguyen, P. H. Estimating configurational entropy of complex molecules: A novel variable transformation approach. *Chemical Physics Letters* **468**, 90–93 (2009). URL <http://linkinghub.elsevier.com/retrieve/pii/S0009261408015807>.
 - [16] Meirovitch, H. Methods for calculating the absolute entropy and free energy of biological systems based on ideas from polymer physics. *Journal of molecular recognition : JMR* **23**, 153–72 (2010). URL <http://www.pubmedcentral.nih.gov/articlerender.fcgi?artid=2823937&tool=pmcentrez&render>
 - [17] King, B. M., Silver, N. W. & Tidor, B. Efficient calculation of molecular configurational entropies using an information theoretic approximation. *The journal of physical chemistry. B* **116**, 2891–904 (2012). URL <http://www.ncbi.nlm.nih.gov/pubmed/22229789>.
 - [18] Reinhard, F. & Grubmüller, H. Estimation of absolute solvent and solvation shell entropies via permutation reduction. *The Journal of chemical physics* **126**, 014102 (2007). URL <http://www.ncbi.nlm.nih.gov/pubmed/17212485>.
 - [19] Wang, L., Abel, R., Friesner, R. a. & Berne, B. J. Thermodynamic properties of liquid water: an application of a nonparametric approach to computing the entropy of a neat fluid. *Journal of chemical theory and computation* **5**, 1462–1473 (2009). URL <http://www.pubmedcentral.nih.gov/articlerender.fcgi?artid=2764996&tool=pmcentrez&render>
 - [20] Gerogiokas, G. *et al.* Prediction of Small Molecule Hydration Thermodynamics with Grid Cell Theory. *Journal of*

- Chemical Theory and Computation* **10**, 35–48 (2014). URL <http://pubs.acs.org/doi/abs/10.1021/ct400783h>.
- [21] Zhang, J. & Liu, J. S. On side-chain conformational entropy of proteins. *PLoS computational biology* **2**, e168 (2006). URL <http://www.pubmedcentral.nih.gov/articlerender.fcgi?artid=1676032&tool=pmcentrez&render>
 - [22] Sciretti, D., Bruscolini, P., Pelizzola, A., Pretti, M. & Jaramillo, A. Computational protein design with side-chain conformational entropy. *Proteins* **74**, 176–91 (2009). URL <http://www.ncbi.nlm.nih.gov/pubmed/18618711>.
 - [23] Frederick, K. K., Marlow, M. S., Valentine, K. G. & Wand, A. J. Conformational entropy in molecular recognition by proteins. *Nature* **448**, 325–329 (2007).
 - [24] Tzeng, S.-R. & Kalodimos, C. G. Protein activity regulation by conformational entropy. *Nature* **19** (2012). URL <http://www.nature.com/doi/finder/10.1038/nature11271>.
 - [25] Karplus, M., Ichiye, T. & Pertirr, B. M. CONFIGURATIONAL ENTROPY OF NATIVE PROTEINS. *Biophysical Journal* **52**, 1083–1085 (1987).
 - [26] Chang, C.-e. & Gilson, M. K. Free Energy, Entropy, and Induced Fit in Host - Guest Recognition: Calculations with the Second-Generation Mining Minima Algorithm. *Journal of American Chemical Society* **126**, 13156–13164 (2004).
 - [27] Kasinath, V., Sharp, K. a. & Wand, a. J. Microscopic insights into the NMR relaxation-based protein conformational entropy meter. *Journal of the American Chemical Society* **135**, 15092–100 (2013). URL <http://www.ncbi.nlm.nih.gov/pubmed/24007504>.
 - [28] Wand, A. J. The dark energy of proteins comes to light: conformational entropy and its role in protein function revealed by {NMR} relaxation. *Current Opinion in Structural Biology* **23**, 75 – 81 (2013). URL <http://www.sciencedirect.com/science/article/pii/S0959440X12001856>. Folding and binding / Protein-nucleic acid interactions.
 - [29] Wang, K., Long, S. & Tian, P. Hierarchical conformational analysis of native lysozyme from sub-millisecond molecular dynamics simulations. *submitted*.
 - [30] Shaw, D. E. *et al.* Atomic-level characterization of the structural dynamics of proteins. *Science (New York, N.Y.)* **330**, 341–6 (2010). URL <http://www.ncbi.nlm.nih.gov/pubmed/20947758>.
 - [31] Zhao, L., Li, W. & Tian, P. Reconciling mediating and slaving roles of water in protein conformational dynamics. *PloS one* **8**, e60553 (2013). URL <http://www.pubmedcentral.nih.gov/articlerender.fcgi?artid=3623917&tool=pmcentrez&render>

- [32] Phillips, J. C. *et al.* Scalable molecular dynamics with namd. *Journal of Computational Chemistry* **26**, 1781–1802 (2005). URL <http://dx.doi.org/10.1002/jcc.20289>.

Figure caption

Figure 1. Analysis of free energy proxies for HEWL based on SCHA conformers with each of 256 backbone dihedrals selected as an order parameter. a) Probability distribution of conformers' statistical weight (defined by the number of snapshots recorded for each conformer); b) Linear correlation coefficient between E_{min}^p and free energy on each of 256 backbone dihedrals, corresponding secondary structures are denoted on the x-axis (α stands for α helix, L stands for loop, β stands for β strand and h stands for 3-10 helix). c) to h), The best (red circles and line) and the worst (blue triangles and line) performance of various energetic and entropic terms as free energy proxies on 256 backbone dihedrals, conformational entropy (S_{conf} , c)), vibrational entropy (S_{vib} , d)), maximum (E_{max}^p , e)), minimum (E_{min}^p , f)), average (E_{avg}^p , g)) and span (E_{span}^p , h)) of protein potential energy. Free energy is based on population distributions and represented as $-\ln N$ with the unit being the gas constant (same for all figures hereafter and in supporting info). i) and j), distributions of linear correlation coefficient (r) between free energy and i) entropic terms (vibrational entropy S_{vib} , conformational entropy S_{conf} and its upperbound $\ln N_{conf}$) (inset is the magnification of the very left part of the plot), j) energetic terms (maximum E_{max}^p , minimum E_{min}^p , average E_{avg}^p and span E_{span}^p of protein potential energy).

Figure 2. Analysis of free energy proxies for HEWL based on SCHA conformers when energetic and entropic terms (conformational entropy S_{conf} and its upperbound $\ln N_{conf}$; vibrational entropy S_{vib} ; maximum E_{max}^p , minimum E_{min}^p , average E_{avg}^p and span E_{span}^p of protein potential energy) are projected onto radius of gyration (R_g in red), number of native contacts (NC in blue) and backbone dihedral distribution based clusters (in cyan).

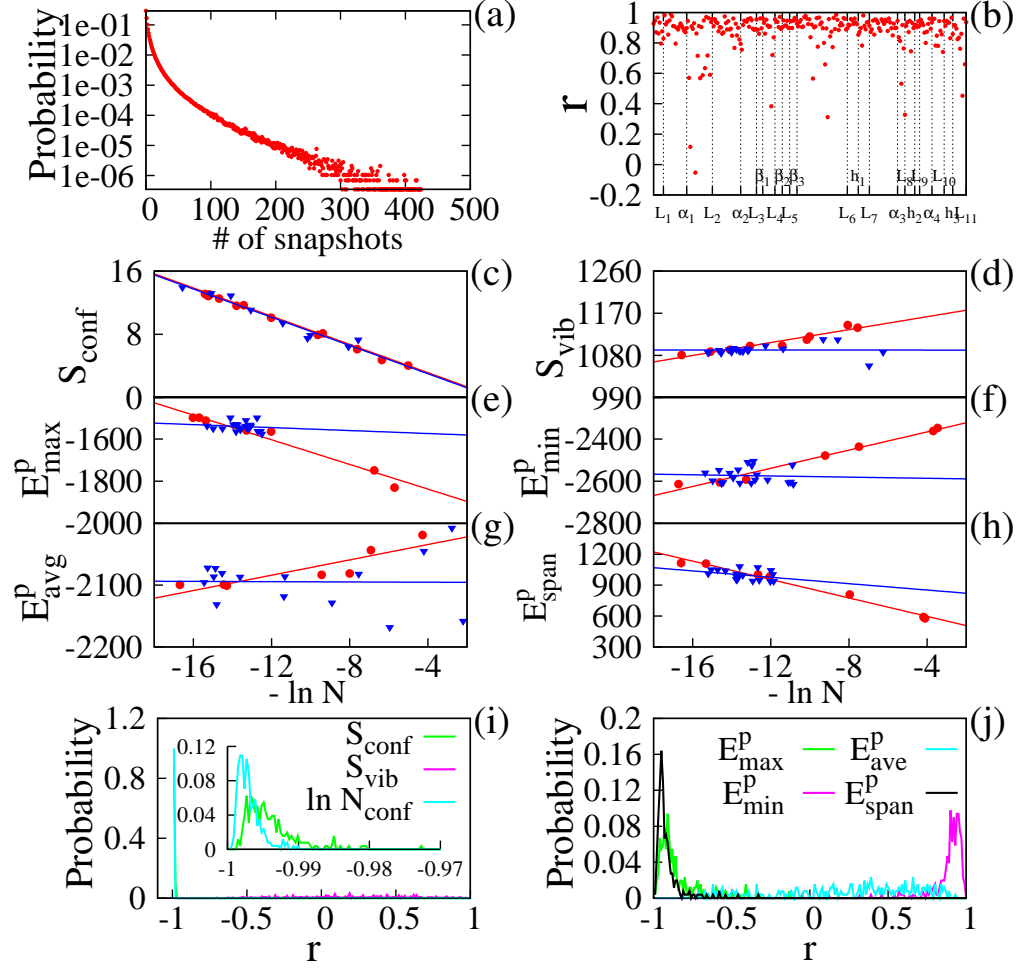


Figure 1

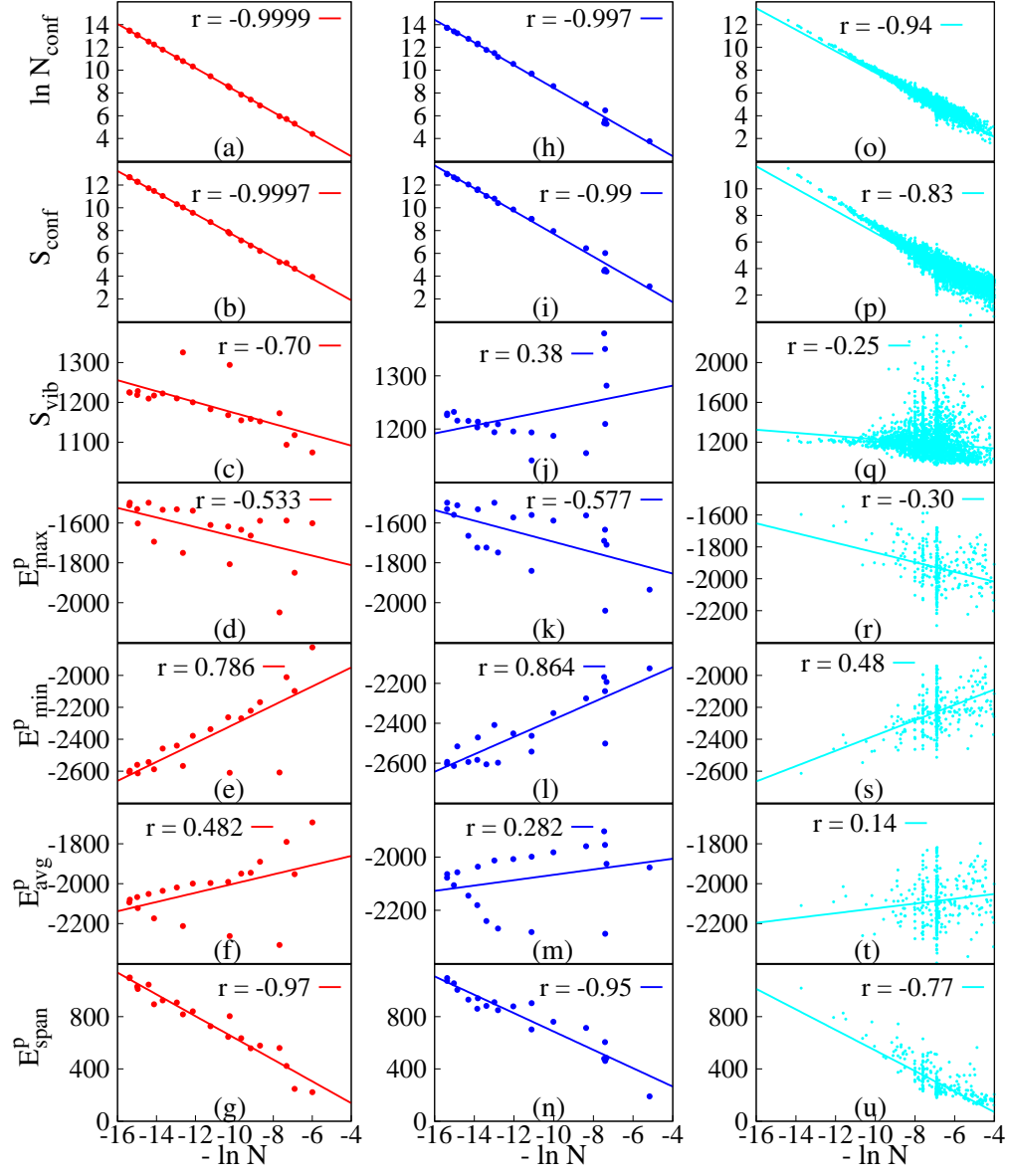


Figure 2

Supporting Information

0.1 Analysis of barstar and ribonuclease trajectories

We analyzed two additional sets of $5\mu s$ MD trajectories of barstar and a ribonuclease[31], where snapshots were written with $1ps$ interval. More heterogeneous life time distributions were observed for conformers (Fig. S1). Nonetheless, equations (5-6) were found to be very good approximations when backbone dihedrals were selected as order parameters. Majority of conformers (3,146,722 out of 3,855,531 for barstar and 2402306 out of 3,257,856 for the ribonuclease) have life time shorter than two intervals.

0.2 Treatment of hydrogen-atom-participating side chain torsional DOFs and backbone torsional DOFs

When non-degenerate torsional DOFs that have participating hydrogen atoms are included to define side-chain-all-atom (SCAA) conformers, the number of involved torsional DOFs increased from 196 to 405 for HEWL and N_{conf} increased nearly two folds (from 2882101 to 5342647). Similar order of correlation strength with free energy is observed for S_{conf} , $\ln N_{conf}$ and S_{vib} on all reaction coordinates analyzed (see Fig. S11). It is noted that projection of potential energy terms is exactly the same for SCAA and SCHA conformers. For the collection of 10- fs resolution HEWL trajectories, the number of four differently defined conformers, include those based on SCHA, SCAA, all-heavy-atom (AHA) and all-atom (AA) torsional DOFs, are 2882101, 5342647, 3782372 and 5423726 respectively. The small difference between the number of SCAA and AA based conformers suggests that backbone torsional state change is well represented by SCAA torsion based conformers. We did not explicitly include backbone torsional states in free energy proxy analysis for the following reasons. Firstly, correlations among backbone torsional DOFs are much stronger than that among side chain torsional DOFs[30, 29], and number of statistically important backbone torsional state combinations is a manageable number to be treated individually[29]. Secondly, in protein folding refinement, design and docking[3, 5], backbone configurations are widely explicitly considered as conformational states that need to have their free energy evaluated. In practice, entropy evaluation based on SCHA torsion may be easily implemented with widely-utilized united-atom model, and SCAA torsion with fully atomic models. Thus naturally form the final two levels of side chain packing.

0.3 Microscopic basis of *enthalpy-centric* and *entropy-centric* algorithms

The canonical configurational integral $Z_N = \int d^{3N}r \exp -\beta U(r)$, with β being the reciprocal temperature and $U(r)$ being the potential energy of the molecular system at configuration r , is the basis for many sampling algorithms. In a naive implementation of the Metropolis algorithm, the integrand (and consequently $U(r)$) is the focus with the implied assumption that the density of states is similar in the whole configurational space, and a significant integrand makes significant contribution to the integral. This is absolutely correct when the sampling is performed over each single possible microstate of the system. Based on correspondence between potential energy of microstates and macroscopic enthalpy, sampling schemes focusing on $U(r)$ is termed *enthalpy-centric* below. In computational treatment of realistic multi-dimensional integral (e.g. partition function of a typical protein molecule), the discretization is rather coarse and a point (i.e. a specific microstates) is utilized to represent a small volume (δv) in the configurational space that may harbor a huge number of conformers. An accurate discretization should be $Z_N = \sum_{\delta v} \sum_{i=1}^{NS_{\delta v}} \exp -\beta U_i$, where the statistical weight of a small volume (δv) in configurational space is dependent upon two factors, the number of microstates ($NS_{\delta v}$) in this volume and potential energies of these microstates ($U_i, i = 1, 2, \dots, NS_{\delta v}$). $NS_{\delta v}$ directly relates to conformational entropy, which is found to be the best proxy of free energy. Algorithms that focusing on the number of available conformers in each visited region of configurational space is termed *entropy-centric* accordingly. Presently, *enthalpy-centric* methodologies dominate and we expect *entropy-centric* development to catch up in the next decade.

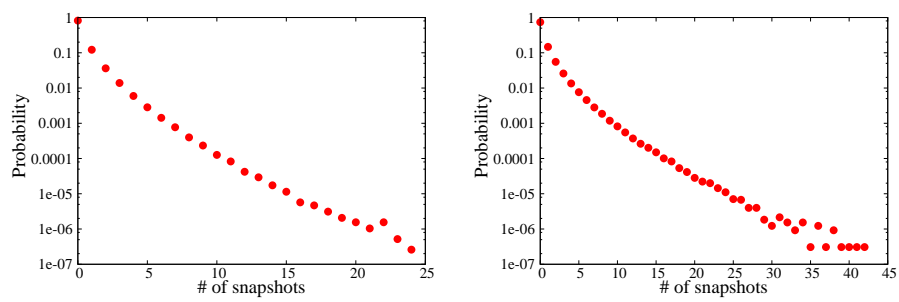


Figure S1: Distribution of statistical weights (represented by number of snapshots) for conformers observed in $5\text{-}\mu\text{s}$ MD trajectories of a)bartar and b)ribonuclease.

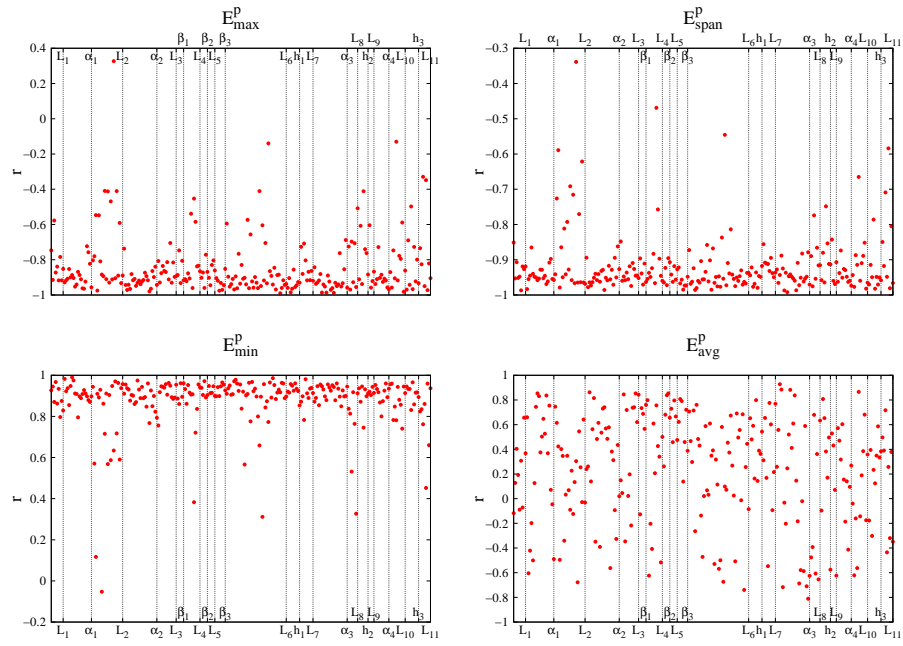


Figure S2. Linear correlation coefficient (r) between E_{\max}^p , E_{\min}^p , E_{avg}^p , E_{span}^p , and free energy on each of 256 HEWL backbone dihedrals, corresponding secondary structures are denoted on the x-axis (α stands for α helix, L stands for loop, β stands for β strand and h stands for 3-10 helix).

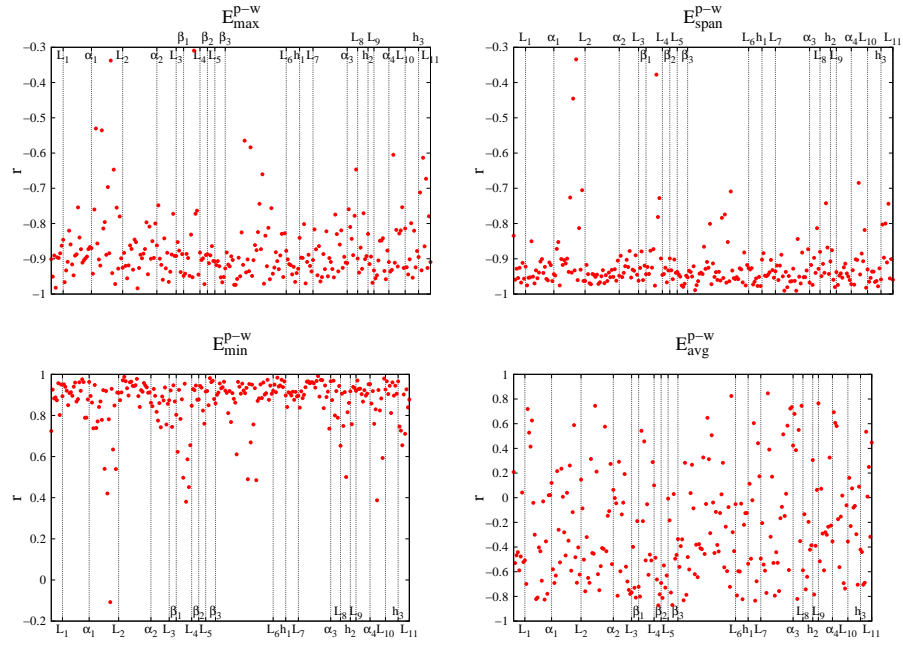


Figure S3. Linear correlation coefficient (r) between E_{max}^{p-w} , E_{min}^{p-w} , E_{avg}^{p-w} , E_{span}^{p-w} and free energy on each of 256 HEWL backbone dihedrals, corresponding secondary structures are denoted on the x-axis (α stands for α helix, L stands for loop, β stands for β strand and h stands for 3-10 helix).

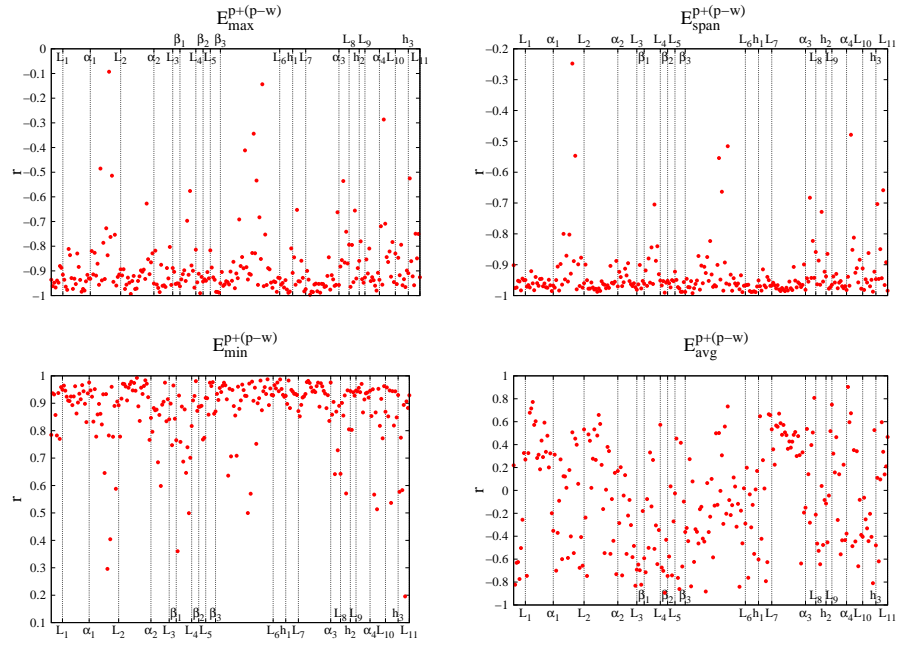


Figure S4. Linear correlation coefficient between $E_{max}^{p+(p-w)}$, $E_{min}^{p+(p-w)}$, $E_{avg}^{p+(p-w)}$, $E_{span}^{p+(p-w)}$ and free energy on each of 256 HEWL backbone dihedrals, corresponding secondary structures are denoted on the x-axis (α stands for α helix, L stands for loop, β stands for β strand and h stands for 3-10 helix).

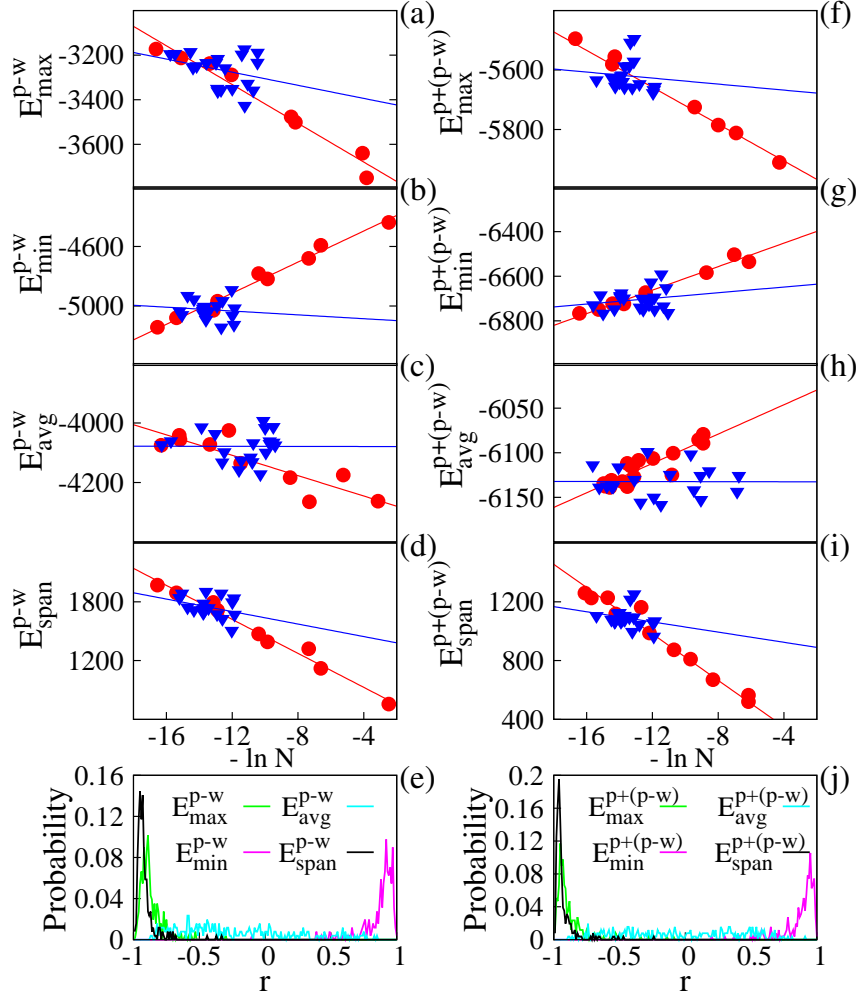


Figure S5. Best (red) and worst (blue) correlations observed on the 256 HEWL backbone dihedrals between (a-d) E_*^{p-w} , (f-i) $E_*^{p+(p-w)}$ and free energy. Distributions of linear correlation coefficient r between e) E_*^{p-w} , j) $E_*^{p+(p-w)}$ and free energy. (* represent *max*, *min*, *avg* or *span*).

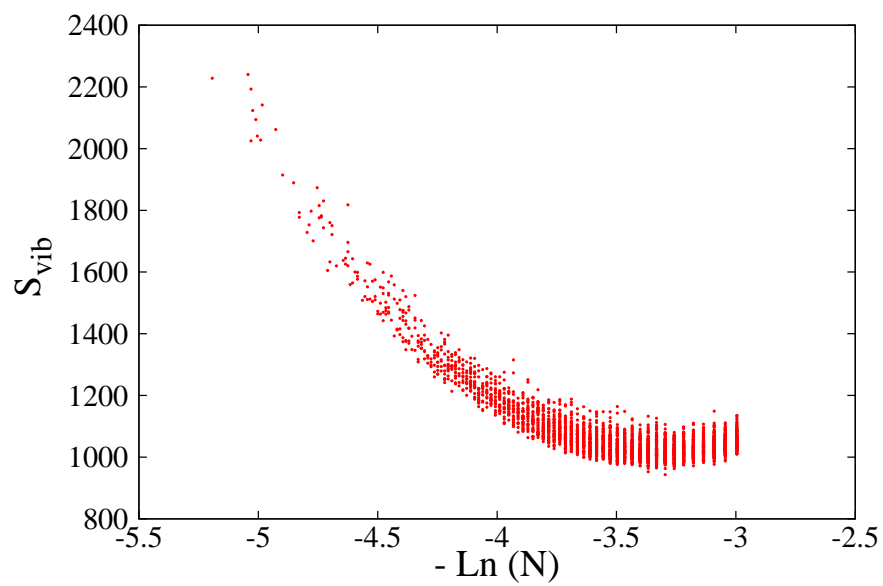


Figure S6. Vibrational entropy S_{vib} vs. free energy (represented by negative natural logarithm of the number of snapshots in each conformer).

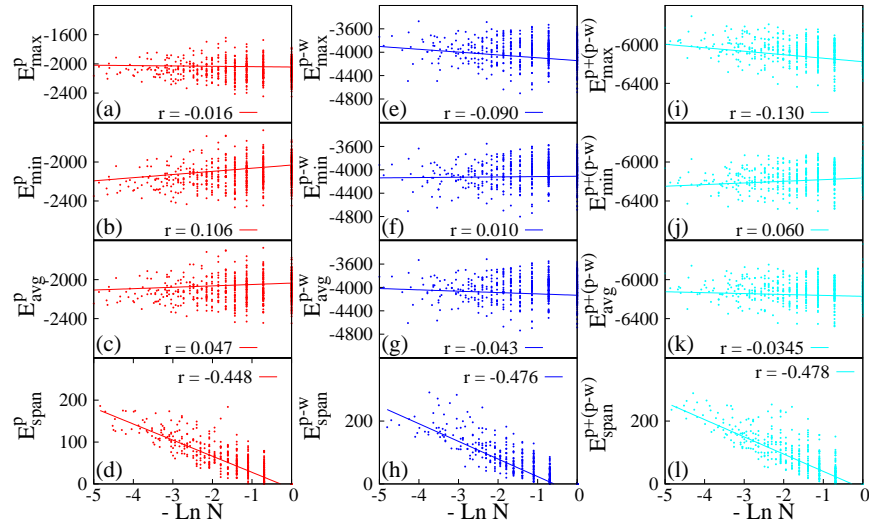


Figure S7. Correlation between various potential energy terms (E_*^p , E_*^{p-w} and E_*^{p+p-w} , with $*$ representing *max*, *min*, *avg* or *span*) and free energy when projected on radius of gyration (red), number of contacts (blue), and backbone dihedral distribution defined clusters (cyan).

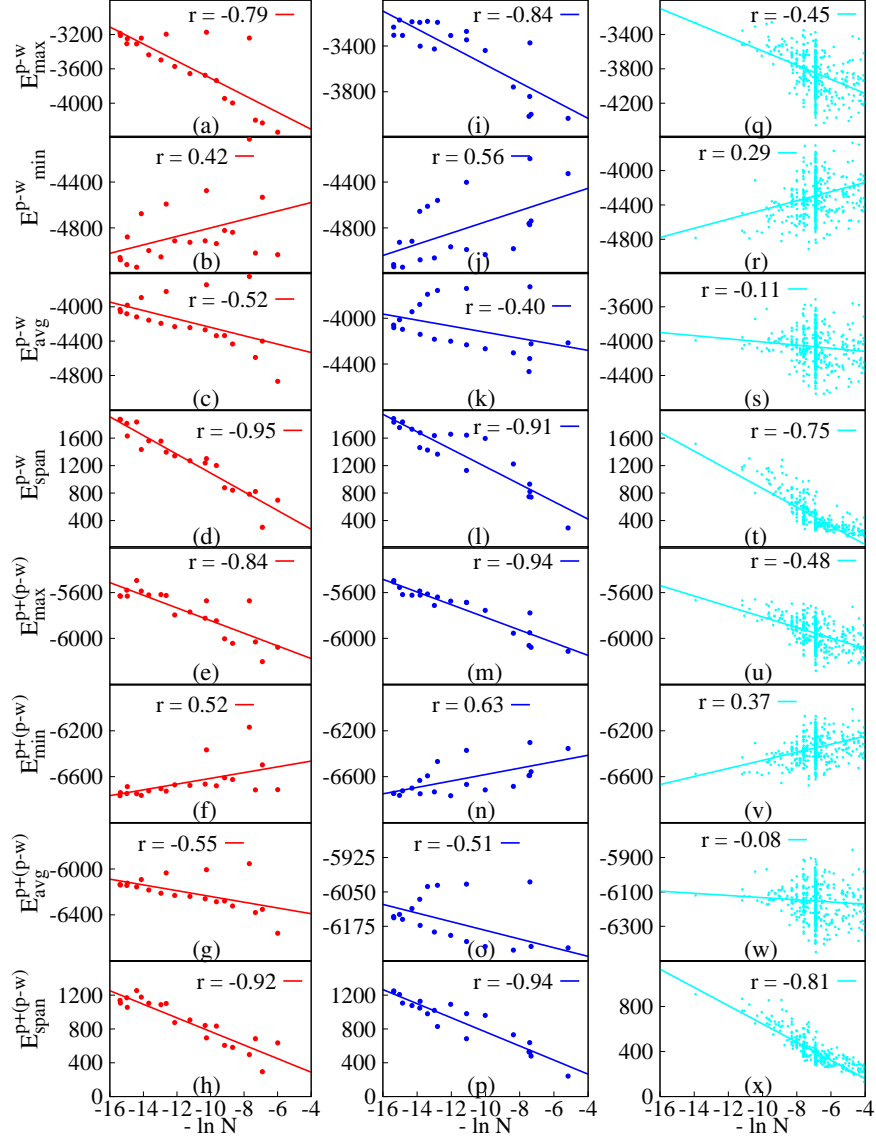


Figure S8. Correlations between free energy and energetic terms (E_*^{p-w} and $E_*^{p+(p-w)}$) when projected on R_g (a-h), NC (i-p) and on backbone distribution defined clusters (q-x). (* represent \max , \min , avg or span).

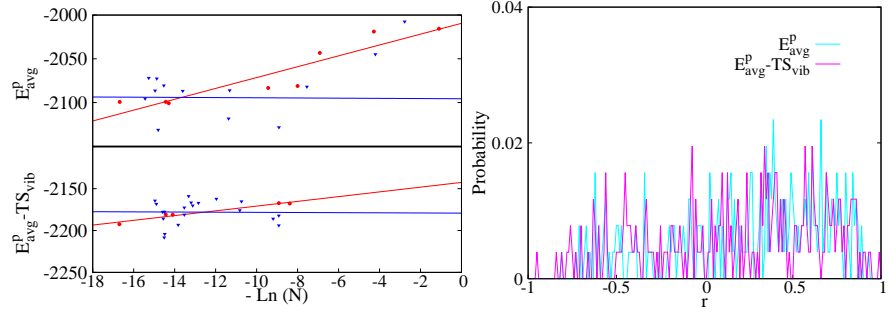


Figure S9. Correlation between free energy and $E_{avg}^* - TS_{vib}$ when 256 backbone dihedrals are selected as order parameters. Left panel: the best (red) and worst (blue) performance of E_{avg}^p , $E_{avg}^p - TS_{vib}$ and $E_{avg}^{p+(p-w)} - TS_{vib}$. Right: the distribution of the linear correlation coefficient r between free energy and E_{avg}^p , $E_{avg}^p - TS_{vib}$ and $E_{avg}^{p+(p-w)} - TS_{vib}$.

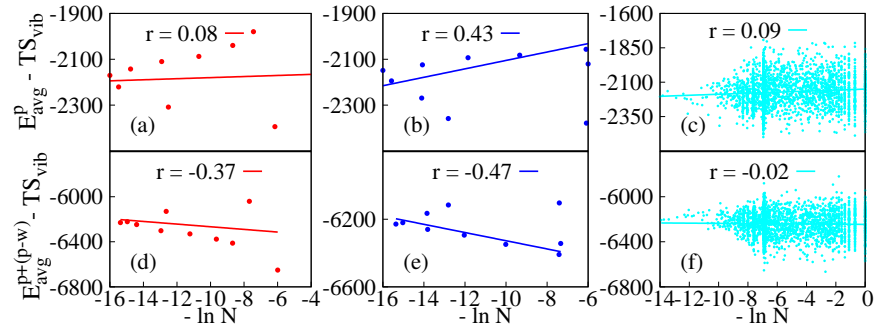


Figure S10. Correlation between free energy and $E_{avg}^p - TS_{vib}$ (upper panels), $E_{avg}^{p+(p-w)} - TS_{vib}$ (lower panels) when R_g (red), NC (blue) and backbone distribution defined clusters (cyan) are selected as order parameters.

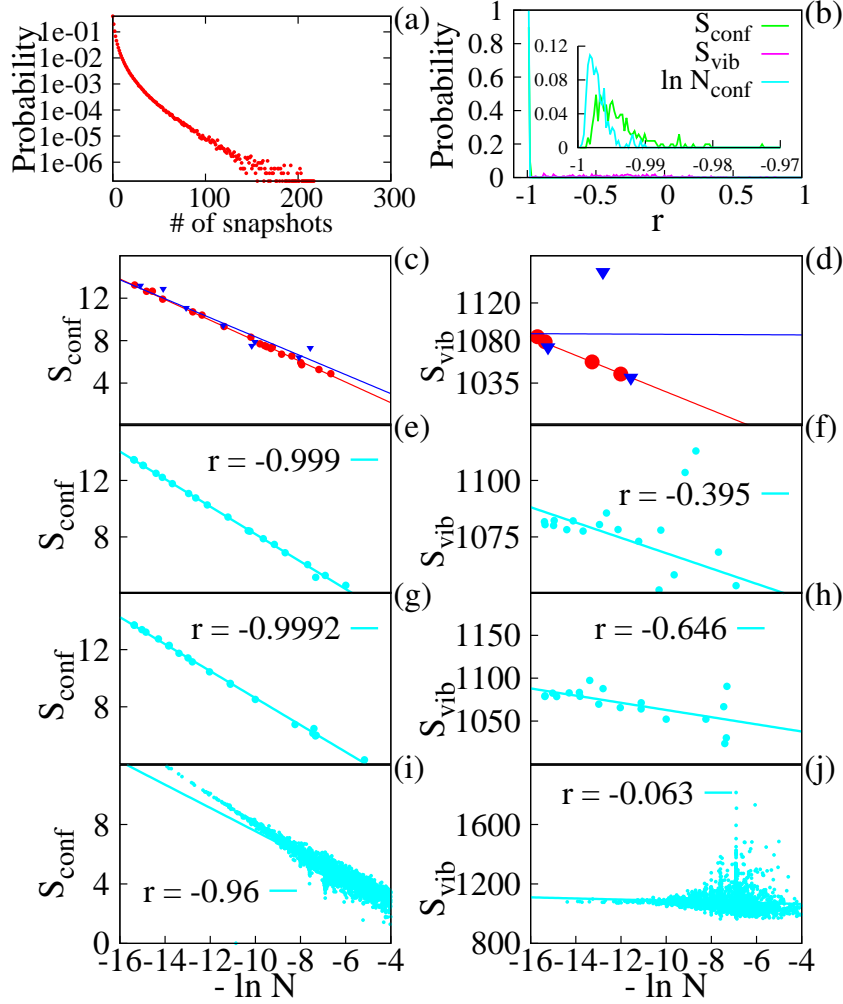


Figure S11. Analysis of a) Distribution of SCAA based conformers' statistical weights (represented by number of snapshots). b) Distributions of linear correlation coefficient r between S_{conf} , S_{vib} , $\ln N_{conf}$ and free energy given SCAA based conformers. (c-d) Best (red) and worst (blue) observed correlations between c) S_{conf} , d) S_{vib} and free energy when 256 backbone dihedrals are selected as order parameters. (e-f) Correlations between e) S_{conf} , f) S_{vib} and free energy when projected on R_g ; (g-h) Correlations between g) S_{conf} , h) S_{vib} and free energy when projected on NC ; (i-j) Correlations between i) S_{conf} , j) S_{vib} and free energy when projected on backbone dihedral distribution defined clusters;